IMAGE QUALITY METRICS FOR SIMILARITY ASSESSMENT IN THE XCT MEASUREMENT OF LATTICE STRUCTURES

Maxwell Praniewicz[1], Jason C. Fox[1]
[1]Engineering Laboratory
National Institute of Standards and Technology
Gaithersburg, Maryland, USA

INTRODUCTION

Lattice structures produced using additive manufacturing (AM) have been investigated by the aerospace and automotive industries because of their light-weighting potential [1–3]. The inspection of these components is often limited to X-ray Computed Tomography (XCT) because their internal features are inaccessible by tactile probes or obscured from optical measurement [4–6]. The capability of XCT to non-destructively resolve a full three-dimensional model of a scanned component has made it a preferred option for the inspection of geometrically complex components [7,8]. However, uncertainty assessment in XCT dimensional measurements of industrial components is currently limited to the substitution method detailed in VDI/VDE 2630-2.1 guideline [9]. This requires similarity between the object to be measured (test object) and a calibrated reference object in terms of material, shape, and size. Producing a reference object similar to an AM lattice structure can be challenging. However, there is no definitive definition of similarity or established limits to which the test object and reference object can vary from one another. Specifically, creating a reference object with similar geometrical complexity and the rough surfaces and form deviations observed in AM components on calibrated surfaces is a non-trivial task and requires the definition of a metric to assess similarity. A previous work by the authors had taken initial steps to understand the limits of similarity by investigating the effect of object dissimilarity on the quality of XCT measurements [10]. Further investigation is needed to determine an appropriate measure for similarity and its relation to dimensional measurements.

In this study, we compare the use of different potential similarity metrics to analyze the varying degrees of similarity between varied XCT scans. Simulated XCT measurements of an array of cylinders conducted in a previous work are further analyzed using several image quality metrics to assess the effect of geometric variations on measurement similarity. A realistic design of a lattice structure is then simulated under degrading XCT scan conditions by manipulating parameters within the simulation to compromise scan quality. The similarity of these simulations is then compared using metrics defined in ASTM E1695 [11], image quality metrics, and dimensional measurements.

METHODOLOGY

Two different sets of experiments are conducted in this work to assess potential similarity metrics. First, previous experimental data is analyzed using new analysis techniques to investigate if there is correlation between previous experimental techniques. Then, new XCT simulations conducted on a lattice geometry are investigated using the described metrics.

Cylinder Array Measurements

In a previous work, XCT simulations of cylinder arrays were investigated using the contrast discrimination function (CDF) described in ASTM E1695 [10]. In this work, three different image quality metrics are used to assess the data and are compared to the previously acquired results. The image quality metrics utilized in this work to compare polychromatic XCT reconstruction slices to monochromatic XCT reconstruction slices are the root-mean-square error (RMSE), the peak signal-to-noise ratio (PSNR), and the structural similarity index (MSSIM). Detailed descriptions of these metrics to analyze XCT slices can be found in Villarraga-Gómez & Smith and are not detailed here for the sake of brevity [12]. These image quality metrics are applied to the material component of the individual cylinders for direct comparison to the results in [10].

Lattice Measurements

A cubic lattice unit cell is created with a cell size of 5 mm, a strut diameter of 1 mm, and patterned to create a 5 x 5 x 5 cubic lattice structure.

Monochromatic and polychromatic XCT acquisitions are simulated using aRTist software [13]. Two additional simulations are performed to examine the effect of projection quality degradation on the resulting reconstruction. In one simulation using the polychromatic spectrum, the focal spot size is increased from a point source to a circular area with a diameter of 0.04 mm, making it slightly larger than the voxel size of 0.0375 mm. In a second additional simulation using the polychromatic spectrum, McRay scatter simulation is enabled in aRTist [14]. Both of these scans are intended to individually introduce common sources of error in XCT image acquisitions. Table 1 details the simulation parameters used in aRTist.

TABLE 1. XCT simulation parameters for lattice structure.

Parameter		Value
Source	Target material	W
	Target angle	45°
	Window material	Be
	Window thickness	0.5 mm
	Acceleration voltage	225 kV
	Current	1 mA
	Physical filter	1.0 mm Cu
	Energy (mono)	103 keV
Detector	Pixel size	0.127 mm
	Number of pixels (WxH)	1536 x 1920
	Source to detector distance	429.76 mm
Object Positioning	Source to rotation axis distance	145.46 mm
Simulation Quality Degradation	Focal spot size	0.04 mm
	Scatter simulation algorithm	McRay
Data Acquisition	Number of projections	1570
	Reconstruction algorithm	FDK
	Bit depth (reconstruction)	32bit

For the analysis, two slices are extracted from all four simulations: monochromatic (Mono.), polychromatic (Poly.), polychromatic with focal spot change (Poly.F), polychromatic with scatter (Poly.S). Slice A, the 961st slice from the bottom of the volume, is the central slice along the vertical axis of the reconstruction and intersected the central plane of the lattice. Slice B, the 1027th slice from the bottom of the volume, is positioned half of a unit cell higher within the volume, intersecting the middle of the vertical struts. This provides a cross section like the cylinder array results, but with greater geometrical complexity. Figure 1 displays the positioning of these two slices on the lattice structure and a cross section view of each slice.

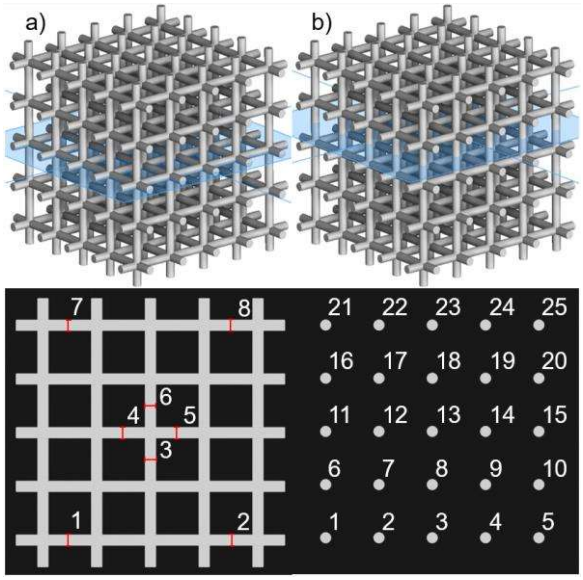

FIGURE 1. Lattice structure used in XCT simulations and position of investigation slices A and B and cross sections at each slice.

Slices A and B are then imported into MATLAB and are background corrected and ISO50 thresholded similar to [10]. The CDF is calculated for all four simulations. The RMSE, PSNR, and MSSIM are calculated for the three polychromatic simulations while using the monochromatic simulations as the reference image. Dimensional measurements of the two different slices are performed as well for all four simulations in VGStudio Max 3.5.2. For slice A, two-point measurements are performed to measure the diameter of struts at select locations. The locations of these two-point measurements and their identifying numbers are shown in Figure 1. For slice B, the circular diameters of all struts are measured within the slice. The identifiers for the struts in slice B are shown in Figure 1. These dimensional measurements are conducted using two different thresholding methodologies as well. An ISO50 method is first utilized for comparison to the results obtained using the different proposed similarity metrics. Second, VGStudio's "advanced surface determination" is used. While this thresholding method makes dimensional measurements less comparable to the similarity

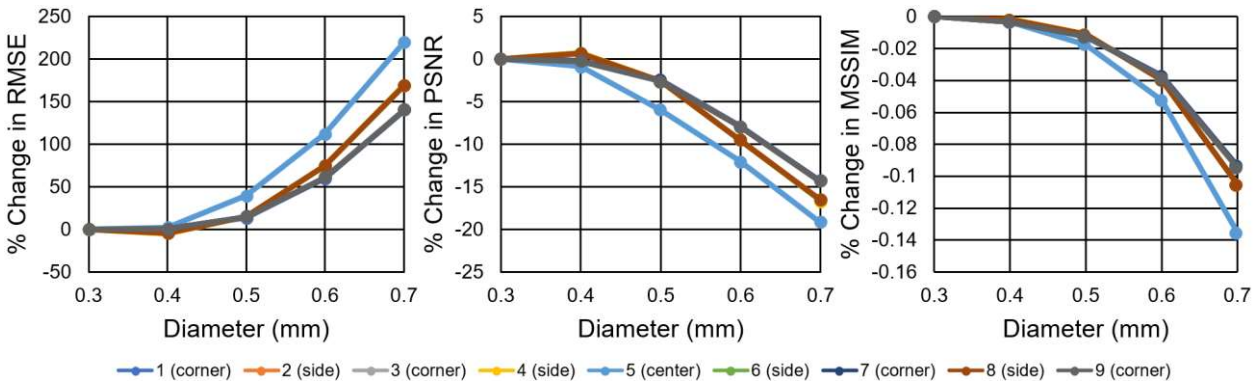

FIGURE 2. Simularity metric results for individual cylinder measurement. Individual curves show the results of image quality metrics on struts 1-9, defined in [10].

metrics obtained using the ISO50 method, this surface determination method is more representative of methods currently used in industry and generally produces more accurate measurements. All dimensional measurements are reported as deviation of the measured diameter from the known lattice strut size of 1 mm.

RESULTS

Cylinder Array Results

Since the image quality calculations are performed on floating-point 32bit values, the exact numeric results of these image quality metrics are largely related to the gray values in the image. Thus, Figure 2 displays the results of the image quality analysis of the cylinder arrays as the percent change in a given metric from the 0.3 mm diameter value. The positions of struts 1-9 are defined in [10]. The results shown here largely follow the trends of results presented in [10]. While the 0.3 mm and 0.4 mm diameter cylinder arrays appear comparable in all metrics, the image quality appears to degrade as the diameter increases. One can also observe that there is variation in the image quality between the different strut locations. The center strut appears to degrade at the highest rate, followed by the side and corner struts. This also agrees with the results reported in [10]. The RMSE appears to have the highest relative change compared to the other two image quality metrics investigated. Comparing the percent change between the 0.3 mm and 0.5 mm for the center cylinder, the RMSE increases by 40% compared to 6% and 0.02% for the PSNR and MSSIM respectively. This higher sensitivity would make it more likely to detect smaller changes in the image, possibly making it a more reliable metric to discern similarity.

Lattice Results

Figures 3 and 4 display the results for the CDF calculations for both slice A and B, respectively.

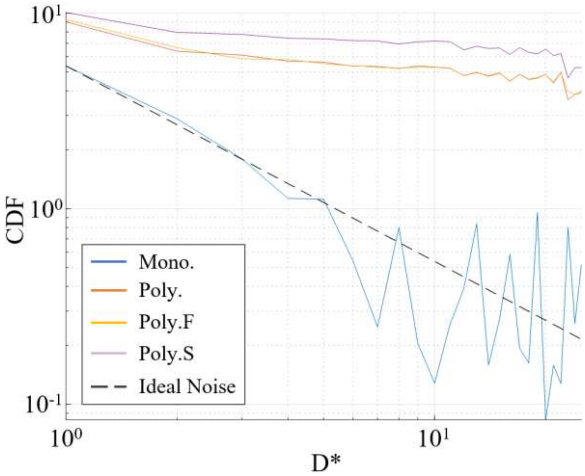

FIGURE 3. CDF calculation of Slice A

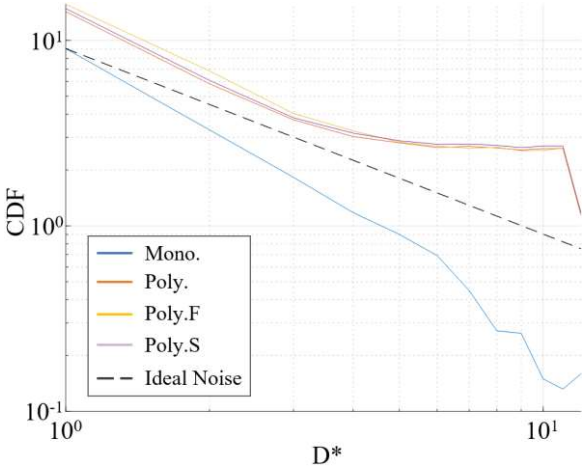

FIGURE 4. CDF calculation of Slice B.

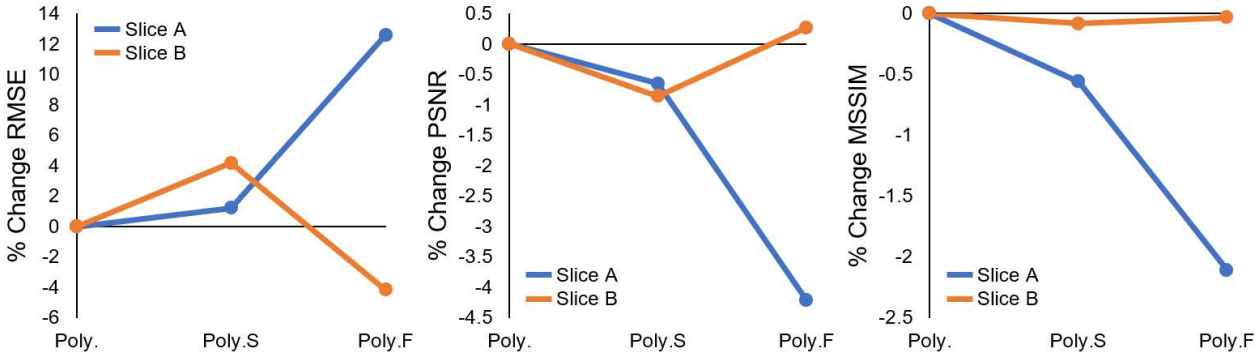

FIGURE 5. Changes in image quaity metrics with variation in XCT scan coniditons.

One can see that the monochromatic simulation in both figures remains around or below the level of statistical noise described in the standard [11]. The exception to this is when D* exceeds 10, where low sample sizes decrease statistical significance in the calculations of the CDF. This was also observed in [10]. In Figure 3, the Poly. and Poly.F CDF curves very closely follow one another, indicating similar levels of noise variation throughout the slice. The Poly.S DFC curve appears to contain a higher mean level of noise in slice A. Conversely, the Poly., Poly.S, and Poly.F CDF curves are much closer in form and mean values in slice B. The Poly. CDF curve has the lowest average value. Unlike Slice A, this is then followed by the Poly.S and Poly.F curves, respectively. Without well-defined confidence intervals, it is difficult to discern whether these curves are in fact dis-similar to one another. However, the large change in mean CDF value in Slice A is not observed in Slice B. This is a marked difference between these two layers, which, if in fact real and not within a confidence overlap of this calculation, would likely be observed by other similarity metrics.

Figure 5 displays the results of the image quality metrics analysis for the 4 different simulations. Similar to Figure 2, these results are presented showing the percentage change between the different simulations using the Poly. results as the baseline for comparison. The results for slice A indicate different trends to those observed in the CDF results. In all three metrics, there is minimal degradation in the image quality with the introduction of scatter. However, the change in focal spot size appears to have had a more significant effect on the image quality. This is opposite the trend identified in the CDF results, indicating that the CDF and the image quality metrics appear to be measuring different phenomena. The results for slice B indicate a very different pattern. The introduction of scatter generally appears to degrade the image quality. However, the increased focal spot size appears to increase the image quality from the baseline Poly. result. These results indicate that variations in XCT parameters can have very different effects on the image quality at different sections of the measurement volume. Thus, the assessment of similarity between different XCT scans may change throughout the measurement volume and should not be limited to a single slice of a reconstruction volume.

The dimensional measurements for slice A are presented in Figure 6. These two-point diameter measurements indicate a trend among the different struts measured. Struts 4 and 5 appear to have the smallest measured diameter for all simulations. Using the advanced surface determination, struts 3 and 6 appear to have the largest diameter. However, the strut diameters generally increase further from the center of the lattice using the ISO50 method. The degradation of the scan quality does appear to influence the diameter measurement. The Mono. simulation produces the smallest diameter measurements in both surface determination methods. The diameters are larger in the Poly. simulation, and

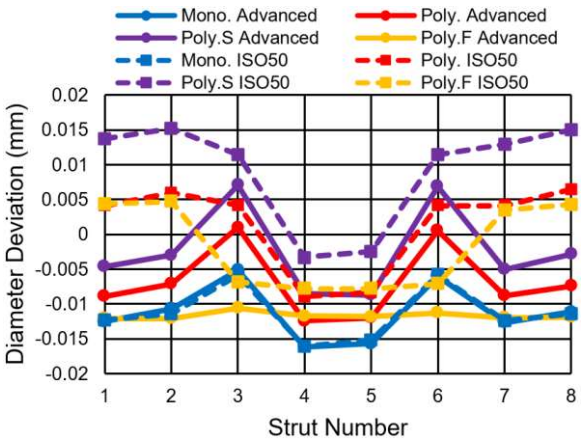

FIGURE 6. Slice A dimensional measurements.

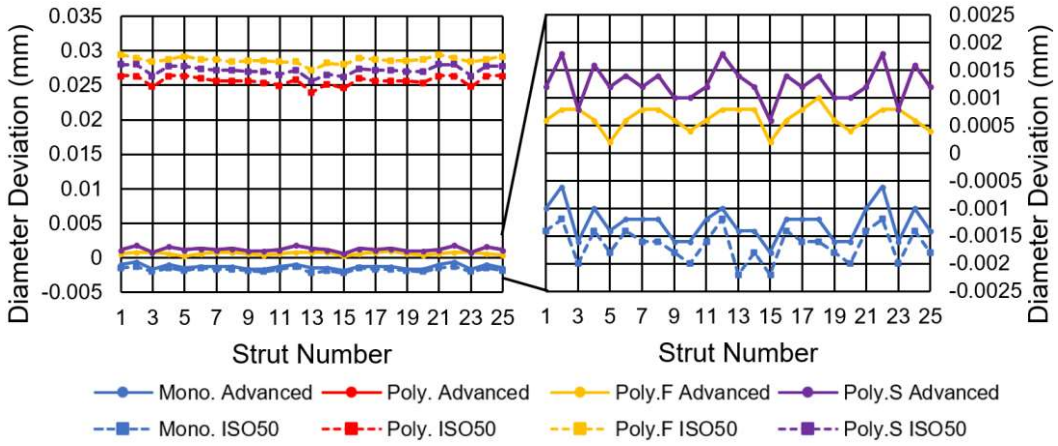

FIGURE 7. Result of dimensional measurement on Slice B. Left image contains all measurements while right displays a smaller range of data for increased clarity.

are increased further by the addition of scatter in Poly.S in both surface determination methods. It appears that introducing scatter creates the large change in these measurements. While this finding agrees with the CDF calculations for slice A, it does not agree with the other image quality metrics results for slice A. The increase in focal spot size appears to decrease the diameter measured in Poly.F in both surface determination methods. However, it is difficult to draw deterministic conclusions from these results, as only one simulation was performed. Thus, there is no indication of the repeatability of these results. Furthermore, all deviations are within 17 µm of the known diameter, which is less than half of the voxel size. Two-point measurement is also an inherently subjective measurement process, so user error should also be considered in these results.

The dimensional measurements for slice B are presented in Figure 7. Clearly, the advanced surface determination provides a more accurate measurement than the IOS50 method. For all polychromatic simulations, the advanced surface determination provides errors almost an order of magnitude lower than the ISO50 method. In the monochromatic simulations, the advanced surface determination method also improved the accuracy for all struts. Examining the advanced surface determination methods closely, one can see that there are slight differences between the simulations. It appears that the addition of scatter in the simulation had no effect on the dimensional measurements using the advanced surface determination. This a conflicting result to those observed in slice A, where the introduction of scatter was shown to increase the measured diameter. The Poly. and Poly.S simulations have the highest average deviations of 1.2 µm. Like the measurements of Slice A, the increase in focal spot size appears to decrease the measured diameter and decreases the variation in the measurements of all struts. However, in the ISO50 results, the increase in focal spot size and scatter both increase the measurement error, with the focal spot size change having the greater effect. This does not appear to follow any of the trends observed in the CDF or the image quality metrics for slice B.

CONCLUSIONS

The ultimate goal of establishing similarity metrics is to broaden the range of traceable dimensional measurements that can be performed with XCT. However, as shown in this work, trends in the explored image quality metrics do not necessarily reflect trends in dimensional measurements. This is also shown to change significantly for different slices within a large measurement volume. The analysis of similarity on a slice-by-slice basis, while rooted in radiographic image analysis, may be a short-sighted approach to analyze XCT data. In this work, the inspected lattice was oriented within the XCT simulation such that the features could be investigated on a slice-by-slice basis. In practice, this is often not the case as many other factors influence the positioning of an object within the measurement volume, such as the consideration of penetration length and cone beam artifacts. Thus, components are often oriented along a coordinate system different to that of reconstruction volume. Measurands often span multiple slices along different orientations, making analysis within a single slice impossible. Hence, it may be better to expand the quantification of similarity to a volumetric

approach. This would not only enable the component to be oriented freely within the reconstruction volume, but would also allow slice by slice changes to be averaged throughout an inspection volume. This would also better coincide with the three-dimensional features commonly analyzed with XCT and would allow greater comparability to real world applications. These volumetric similarity metrics will be the subject of future research.

DISCLAIMER

Official contribution of the National Institute of Standards and Technology (NIST); not subject to copyright in the USA. The full descriptions of the procedures used in this paper require the identification of certain commercial products. The inclusion of such information should in no way be construed as indicating that such products are endorsed by NIST or are recommended by NIST or that they are necessarily the best materials, instruments, software, or suppliers for the purposes described.

REFERENCES

[1] "Roadmap for Automotive Additive Manufacturing," United States Council for Automotive Research LLC, 2021.

[2] L.-Y. Chen, S.-X. Liang, Y. Liu, and L.-C. Zhang, "Additive manufacturing of metallic lattice structures: Unconstrained design, accurate fabrication, fascinated performances, and challenges," *Materials Science and Engineering: R: Reports*, vol. 146, p. 100648, Oct. 2021, doi: 10.1016/j.mser.2021.100648.

[3] B. Blakey-Milner *et al.*, "Metal additive manufacturing in aerospace: A review," *Materials & Design*, vol. 209, p. 110008, Nov. 2021, doi: 10.1016/j.matdes.2021.110008.

[4] M. Dallago, B. Winiarski, F. Zanini, S. Carmignato, and M. Benedetti, "On the effect of geometrical imperfections and defects on the fatigue strength of cellular lattice structures additively manufactured via Selective Laser Melting," *International Journal of Fatigue*, vol. 124, pp. 348–360, 2019, doi: https://doi.org/10.1016/j.ijfatigue.2019.03.019.

[5] B. Lozanovski *et al.*, "Non-destructive simulation of node defects in additively manufactured lattice structures," *Additive Manufacturing*, vol. 36, p. 101593, Dec. 2020, doi: 10.1016/j.addma.2020.101593.

[6] A. du Plessis, G. Schwaderer, I. Cristofolini, M. Zago, and M. Benedetti, "Dimensional metrology of additively manufactured lattice structures by combined tactile probe and X-ray tomography," *Material Design & Processing Communications*, vol. n/a, no. n/a, 2020, doi: https://doi.org/10.1002/mdp2.216.

[7] R. K. Leach, D. Bourell, S. Carmignato, A. Donmez, N. Senin, and W. Dewulf, "Geometrical metrology for metal additive manufacturing," *CIRP Annals*, vol. 68, no. 2, pp. 677–700, 2019, doi: https://doi.org/10.1016/j.cirp.2019.05.004.

[8] A. Thompson, I. Maskery, and R. K. Leach, "X-ray computed tomography for additive manufacturing: a review," *Measurement Science and Technology*, vol. 27, no. 7, Art. no. 7, Jul. 2016, doi: Artn 072001 10.1088/0957-0233/27/7/072001.

[9] Verein Deutscher Ingenieure (VDI), "VDI/VDE 2630 Blatt 2.1 Computed tomography in dimensional measurement: Determination of the uncertainty of measurement and the test process suitability of coordinate measurement systems with CT sensors," Düsseldorf, Germany, 2015.

[10] M. Praniewicz, M. Ferrucci, J. Fox, and C. Saldana, "Testing the similarity conditions in the CT measurement of additively manufactured lattice structures," presented at the Joint Special Interest Groupe meeting between euspen and ASPE, Advancing Precision in Additive Manufacturing, Oct. 2021. Accessed: Oct. 19, 2021. [Online]. Available: https://www.nist.gov/publications/testing-similarity-conditions-ct-measurement-additively-manufactured-lattice-structures

[11] ASTM International, "ASTM E1695 - 20: Standard Test Method for Measurement of Computed Tomography (CT) System Performance," ASTM International, West Conshohocken, PA, 2020.

[12] H. Villarraga-Gómez and S. T. Smith, "Effect of the number of projections on dimensional measurements with X-ray computed tomography," *Precision Engineering*, vol. 66, pp. 445–456, Nov. 2020, doi: 10.1016/j.precisioneng.2020.08.006.

[13] C. Bellon, A. Deresch, C. Gollwitzer, and G.-R. Jaenisch, "Radiographic simulator aRTist: version 2," 2012.

[14] C. Bellon, A. Deresch, and G.-R. Jaenisch, “Radiography Simulation with aRTist – Combining Analytical and Monte Carlo Methods,” Ghent, Belgium, 2015.